

---

# On the Autocorrelation, LCR and AFD of the 802.11n/ac Fading Channel Models

Gonçalo N. Tavares

January, 2016

---

Gonçalo N. Tavares is with the Department of Electrical and Computer Engineering, Instituto Superior Técnico (IST) and with Instituto de Engenharia de Sistemas e Computadores — Investigação e Desenvolvimento (INESC-ID), Lisbon, Portugal (email: [goncalo.tavares@inesc-id.pt](mailto:goncalo.tavares@inesc-id.pt)).

## **Important notice**

To the best of the author's knowledge, the results in this report are correct and accurate. However and due to the its preliminary status, some errors may still subsist. Permission to use the results in this report is granted provided the results are duly acknowledged and referenced.

# Abstract

In this report, we present closed-form expressions for the complex autocorrelation function (ACF) and for the envelope level crossing rate (LCR) and average fade duration (AFD) parameters pertaining to the fading channel models proposed in the IEEE 802.11n/ac standards, which specify a bell-shaped Doppler power spectral density (PSD), truncated to a maximum cut-off frequency  $f_{max}$ . It is shown that the ACF is not very sensitive to  $f_{max}$  and that the dependence of the LCR and AFD on this parameter may be exploited to ease the implementation of practical channel simulators for this standard. A new general series expansion for the LCR of Rice-distributed envelopes, which avoids numerical integration, together with an useful upper bound on the absolute relative error (i.e., precision) of the truncated series is also presented and analyzed.

**Keywords:** Wireless WANs, IEEE 802.11n/ac, complex autocorrelation, Level crossing rate, average fade duration, Gaussian random vector, fading channel simulation.



# Contents

Abstract . . . . .	i
Contents . . . . .	iii
1 Introduction . . . . .	1
2 Exact expression for the autocorrelation . . . . .	3
2.1 Results and discussion . . . . .	4
3 Level Crossing Rate and Average Fade Duration . . . . .	6
3.1 LCR error characterization . . . . .	9
3.2 AFD error characterization . . . . .	11
3.3 Results and discussion . . . . .	11
4 Conclusions . . . . .	17
A.1 Analysis for $f_{max} > \beta \geq 0$ . . . . .	19
A.2 Analysis for $0 < f_{max} \leq \beta$ . . . . .	22
A.3 The case when $\gamma \leq 0$ and/or $\beta < 0$ and/or $\tau < 0$ . . . . .	22
A.4 Summary . . . . .	22
Appendix A – Derivation of $I(\tau, \alpha, \beta, \gamma)$ in closed-form . . . . .	19
Appendix B – Derivation of series expansion for the LCR . . . . .	25
References . . . . .	27



# 1 Introduction

Wireless local area networks (WLANs) based on the IEEE 802.11 standards are now widely deployed and have become near-ubiquitous. Starting with the 802.11n amendment, the standard supports the use of multiple-input, multiple output (MIMO) technology using up to  $M$  transmit and  $N$  receive antennas ( $M, N = 4$ , for 802.11n [1] and  $M, N = 8$  for 802.11ac [2]) and specifies six slow-fading tapped delay line channel models (A-F) with delay spreads ranging from 0 (flat-fading) to 150 ns. These models will also be adopted as indoor channel models in the future 802.11ax amendment [3] which is expected to provide a theoretical four-fold throughput increase relative to 802.11ac. Further discussion of this standard is kept at the minimum required to allow a self-contained explanation of the results. For a detailed description of the 802.11n/ac amendments the reader is referred to [1–4] and to the references therein. Assuming transmission over a quasi-static time-dispersive fading channel, the received  $N \times 1$  complex signal vector may be expressed as [5]

$$\mathbf{r}(t) = \sum_{l=0}^{L-1} \mathbf{H}_l(t) \mathbf{x}(t - \tau_l) + \mathbf{n}(t) \quad (1)$$

where  $L$  is the number of channel taps each with delay  $\tau_l$ ,  $\mathbf{H}_l(t)$  is the  $N \times M$   $l$ -th tap MIMO channel matrix,  $\mathbf{x}(t)$  is the  $M \times 1$  transmitted signal vector, and  $\mathbf{n}(t)$  an  $N \times 1$  additive Gaussian zero-mean complex noise vector. For the  $l$ -th tap, the channel matrix is determined as [1]

$$\mathbf{H}_l(t) = \sqrt{P_l} \left( \sqrt{\frac{K_l}{K_l + 1}} \mathbf{H}^{\text{LOS}}(t) + \sqrt{\frac{1}{K_l + 1}} \mathbf{H}_l^{\text{NLOS}}(t) \right) \quad (2)$$

where  $P_l$  is the tap total power,  $K_l$  is the tap Rice factor (ratio between the specular and the scattered power),  $\mathbf{H}^{\text{LOS}}(t)$  is a deterministic (constant channel) matrix representing the effect of line-of-sight (LOS) propagation and  $\mathbf{H}_l^{\text{NLOS}}(t)$  is a random (scattered channel) matrix modeling the effect of non line-of-sight (NLOS) propagation, the elements of which are complex-valued, correlated, zero-mean, unit variance Gaussian random variables. To induce the desired MIMO spatial correlation, a tap-wise Kronecker model is used with the NLOS matrix determined as [1]  $\mathbf{H}_l^{\text{NLOS}}(t) = \text{unvec} \left( (\mathbf{R}_l^{\text{RX}} \otimes \mathbf{R}_l^{\text{TX}})^{\frac{1}{2}} \text{vec}(\mathbf{H}_{iid}(t)) \right)$  where  $\mathbf{R}_l^{\text{TX}}$  and  $\mathbf{R}_l^{\text{RX}}$  are  $M \times M$  and  $N \times N$  transmit and receive correlation matrices respectively,  $(\mathbf{R})^{\frac{1}{2}}$  stands for the Cholesky decomposition of the positive-definite matrix  $\mathbf{R}$ ,  $(\cdot)^T$  stands for vector or matrix transpose,  $\mathbf{H}_{iid}(t)$  is an  $N \times M$  matrix of complex-valued, independent, zero-mean, unit-variance Gaussian random variables,  $\otimes$  is the Kronecker product,  $\text{vec}(\cdot)$  is the column stacking operator which stacks the  $M$  columns of an  $N \times M$  matrix sequentially into a  $NM \times 1$  column vector and  $\text{unvec}(\cdot)$  is the inverse  $\text{vec}(\cdot)$  operation. The channel matrix evolves over time, modeling the

effect of the time-selectivity of the fading channel. It assumes that both transmitter and receiver are stationary and that human-based and vehicle movement in between induces a Doppler effect with power spectral density (PSD) given by<sup>1</sup>

$$S(f) = \begin{cases} \frac{K_0}{f_d} \left[ \frac{1}{1+A\left(\frac{f}{f_d}\right)^2} + \overbrace{\frac{B}{1+C\left(\frac{f-f_{spike}}{f_{spike}}\right)^2}}^{\text{Model F only}} \right], & |f| \leq f_{max} \\ 0, & |f| > f_{max} \end{cases} \quad (3)$$

where  $A = 9$ ,  $B = 0.5$  and  $C = 90000$  [1]. The Doppler frequency  $f_d$  is given by  $f_d = \frac{v_0}{c} f_c$  where  $v_0$  is the speed of people moving between the transmitter and receiver ( $v_0 = 1.2$  km/h for 802.11n and  $v_0 = 0.089$  km/h for 802.11ac) and  $f_c$  is the carrier frequency (either  $f_c = 2.4$  GHz or  $f_c = 5.25$  GHz). This Doppler component is present in all models. For channel model F, an additional Doppler component is included to model the effect of a moving vehicle. The Doppler frequency of this component is  $f_{spike} = \frac{v_1}{c} f_c$  where  $v_1 = 40$  km/h is the speed of the vehicle. The frequency  $f_{max}$  is the Doppler spectrum cut-off frequency and its value is set somewhat arbitrarily at  $f_{max} = 5f_d$  [1, Sec. 4.7.1] for models A-E. For model F, this frequency is set approximately at  $f_{max} = 40f_d = 1.2f_{spike}$ , as can be inferred from [1, Fig. 6]. The factor  $K_0/f_d$  has been introduced in (3) to render  $S(f)$  dimensionally correct ( $K_0$  is expressed in Watt) and also to allow the total power  $\int_{-\infty}^{\infty} S(f) df$  to be set arbitrarily.

Let us consider the simulation of one channel tap of any of the 802.11n/ac channel models for a period with duration  $T_0$  second. From the previous discussion, we conclude that, for each channel tap, this requires the generation of  $NM$  independent Gaussian random processes  $h_{ij}(t)$ ,  $i = 0, \dots, N-1$ ,  $j = 0, \dots, M-1$ ,  $0 < t \leq T_0$  [i.e., one process for each element of  $\mathbf{H}_l(t)$ ], each exhibiting the desired autocovariance given by the inverse Fourier transform of the PSD in (3). Let  $h(t) \triangleq z(t) + \mu$  denote any of the stationary baseband complex fading signals  $h_{ij}(t)$ , where  $z(t) = x(t) + jy(t)$  is a zero mean, stationary, circularly symmetric complex Gaussian process with real and imaginary components  $x(t)$  and  $y(t)$  respectively, with equal variances  $\sigma_x^2 = \sigma_y^2 \triangleq b_0$  and  $\mu \triangleq E[h(t)]$  is the complex mean value of  $h(t)$ . The autocovariance of  $h(t)$  is defined as  $C_{hh}(\tau) \triangleq E[(h(t) - \mu)^*(h(t+\tau) - \mu)] = R_{hh}(\tau) - |\mu|^2$  where  $R_{hh}(\tau) \triangleq E[h^*(t)h(t+\tau)]$  is the autocorrelation of  $h(t)$ . The envelope of  $h(t)$  is the process  $H(t) \triangleq |h(t)|$  which is either Rayleigh-distributed if  $\mu = 0$  or Rice-distributed if  $\mu \neq 0$ . The total power of  $h(t)$  is  $\Omega \triangleq R_{hh}(0) = 2b_0 + |\mu|^2$  and the Rice factor is  $K \triangleq \frac{|\mu|^2}{2b_0}$ .

The purpose of this report is to present a closed-form expression for the autocorrelation of  $z(t)$ , hereafter denoted  $R(\tau)$ , and also for the level crossing rate (LCR) and average fade

---

<sup>1</sup>Note that the PSD in (3) does not include the specular component.



duration (AFD) of the envelope of the fading process  $h(t)$ . A new expansion for the LCR of general Rician fading envelopes which avoids numerical integration, is also presented. These expressions, which, to the author's knowledge, have not yet appeared in the open literature, are useful for assessing the quality of fading channel simulators for the 802.11n/ac standards.

## 2 Exact expression for the autocorrelation

The autocorrelation function (ACF) corresponding to the spectrum (3) is obtained by taking its inverse Fourier transform  $R(\tau) = \int_{-f_{max}}^{f_{max}} S(f) e^{j2\pi f\tau} df$ . For finite  $f_{max}$ ,  $R(\tau)$  may be obtained from the general definite integral  $I(\tau, \alpha, \beta, \gamma) \triangleq \int_{-f_{max}}^{f_{max}} \frac{e^{j2\pi f\tau}}{1 + \alpha \left(\frac{f-\beta}{\gamma}\right)^2} df$ . Factoring the integrand denominator and using complex integration, it is shown in Appendix A that, for  $\alpha, \gamma > 0$  and  $f_{max} > \beta \geq 0$

$$I(\tau, \alpha, \beta, \gamma) = \begin{cases} \frac{\gamma}{2\sqrt{\alpha}} e^{j2\pi\beta\tau} \left( F(z_+\tau) - F(-z_+^*\tau) - F(z_-^*\tau) + F(-z_-\tau) + 2\pi e^{-2\pi \frac{\gamma}{\sqrt{\alpha}}|\tau|} \right), & \tau \neq 0 \\ \frac{\gamma}{\sqrt{\alpha}} \left[ \arctan \left( \sqrt{\alpha} \frac{f_{max}-\beta}{\gamma} \right) + \arctan \left( \sqrt{\alpha} \frac{f_{max}+\beta}{\gamma} \right) \right], & \tau = 0 \end{cases} \quad (4)$$

where  $(\cdot)^*$  denotes complex conjugate;  $z_{\pm} \triangleq \frac{\gamma}{\sqrt{\alpha}} + j(f_{max} \pm \beta)$  and  $F(u) \triangleq j e^{2\pi \Re\{u\}} E_1(2\pi u)$  where  $\Re\{\cdot\}$  stands for real part and  $E_1(u)$  is the complex exponential integral defined as<sup>2</sup> [6, eq (5.1.1)]  $E_1(z) \triangleq \int_z^{\infty} \frac{e^{-t}}{t} dt, |\arg\{z\}| < \pi, z \neq 0 + j0$ . It is useful to note that because  $E_1^*(u) = E_1(u^*)$ , then  $F^*(u) = -F(u^*)$ . Using (3) and (4), the ACF for finite  $f_{max}$  may be expressed as:

$$\begin{aligned} R(\tau) &= \frac{K_0}{f_d} [I(\tau, A, 0, f_d) + B I(\tau, C, f_{spike}, f_{spike})] \\ &= \frac{K_0}{\sqrt{A}} \left( \Re \{ F(z_0\tau) + F(-z_0^*\tau) \} + \pi e^{-2\pi \frac{f_d}{\sqrt{A}}|\tau|} \right) \\ &\quad + \frac{K_0 B}{2\sqrt{C}} \frac{f_{spike}}{f_d} e^{j2\pi f_{spike}\tau} \left( F(z_+\tau) - F(-z_+^*\tau) - F(z_-^*\tau) + F(-z_-\tau) + 2\pi e^{-2\pi \frac{f_{spike}}{\sqrt{C}}|\tau|} \right) \end{aligned} \quad (5)$$

where  $z_0 \triangleq \frac{f_d}{\sqrt{A}} + j f_{max}$  and now  $z_{\pm} \triangleq \frac{f_{spike}}{\sqrt{C}} + j(f_{max} \pm f_{spike})$ . For  $\tau = 0$ , the ACF is

$$R(0) = K_0 \left( \frac{2}{\sqrt{A}} \arctan \left( \sqrt{A} \xi_d \right) + \frac{B \xi_0}{\sqrt{C}} \left[ \arctan \left( \sqrt{C} (\xi_s - 1) \right) + \arctan \left( \sqrt{C} (\xi_s + 1) \right) \right] \right) \quad (6)$$

where  $\xi_0 \triangleq \frac{f_{spike}}{f_d}$ ,  $\xi_d \triangleq \frac{f_{max}}{f_d}$  and  $\xi_s \triangleq \frac{f_{max}}{f_{spike}}$  have been defined for convenience [see Appendix A for a justification of the first term in (5) and (6)].

---

<sup>2</sup>A closely related function (also known as complex exponential integral) is defined as  $E_i(z) \triangleq -\int_{-z}^{\infty} \frac{e^{-t}}{t} dt, |\arg\{-z\}| < \pi, z \neq 0 + j0$  [6]. A simple relation between these functions is [7, eq. (9)]  $E_1(z) = -E_i(-z) - j\pi \text{sign}(\arg\{z\})$  with the **sign** function defined as  $\text{sign}(x) \triangleq \begin{cases} x/|x|, & x \neq 0 \\ 0, & x = 0 \end{cases}$ .

Since the special function  $E_1(z)$  is readily available in most mathematical software packages (e.g., *Matlab*, *Mathematica*, *Maple*) and can be computed with arbitrary numerical precision, equations (5) and (6) are useful to determine  $R(\tau)$  for any set of parameters, including  $f_{max}$ , without the need for custom numerical integration. The computation of special functions in these packages is usually highly optimized and permits computation of (5) with a precision and speed that is difficult to attain using a custom integration routine. When  $f_{max} \rightarrow \infty$ ,  $z_0$  and  $z_{\pm}$  approach  $j\infty$  and all the functions  $F(\cdot)$  approach zero. Therefore

$$R(\tau)|_{f_{max}=\infty} = \frac{K_0\pi}{\sqrt{A}} e^{-2\pi\frac{f_d}{\sqrt{A}}|\tau|} + \frac{K_0\pi B}{\sqrt{C}} \frac{f_{spike}}{f_d} e^{j2\pi f_{spike}\tau} e^{-2\pi\frac{f_{spike}}{\sqrt{C}}|\tau|}$$

which could be obtained by inverse Fourier transforming  $S(f)$  in (3) with  $f_{max} = \infty$ .

## 2.1 Results and discussion

In this Section, several numerical results pertaining to the complex autocorrelation using the proposed computational expressions are presented. For brevity, all the results consider only the 802.11n channel F parameters with  $f_c = 2.4$  GHz ( $f_d = 2.667$  Hz,  $f_{spike} = 88.89$  Hz). For 802.11n with  $f_c = 5.25$  GHz and also for 802.11ac with both carrier frequencies, the corresponding results are qualitatively similar.

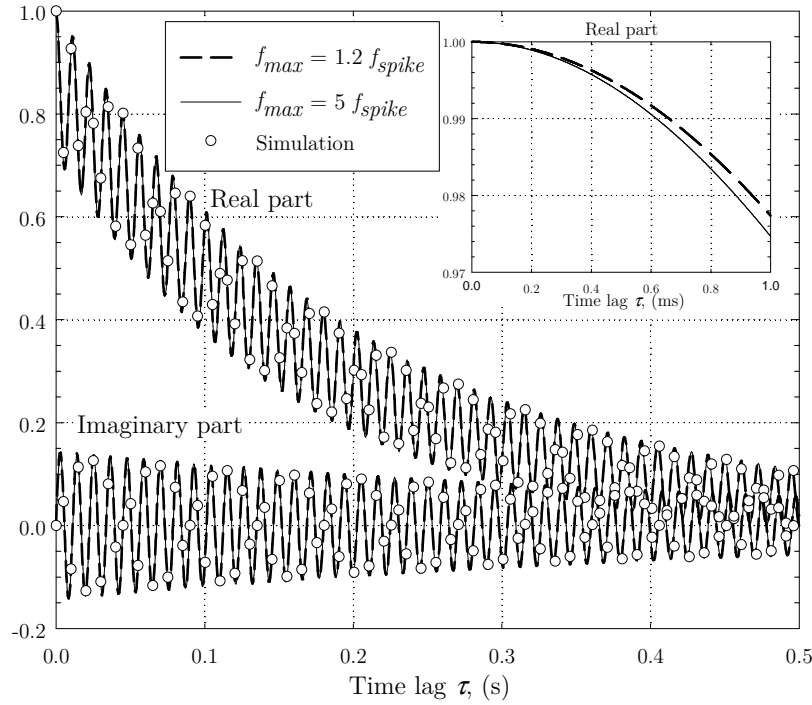


**Figure 1:** Complex autocorrelation  $R(\tau)$  for model F (normalized).

Fig. 1 presents the autocorrelation  $R(\tau)$  computed from (5) with  $f_{max} = 1.2f_{spike}$  and also with  $f_{max} = 5f_{spike}$ . The circles in figures in this report represent simulation results using

the two, seventh-order, infinite impulse response (IIR) filters proposed in [8] for both channel models A-E and F, which are hard-coded for a sampling frequency  $f_s = 300f_d$  and for a cut-off frequency  $f_{max} = 5f_d$  for models A-E and  $f_{max} = 40f_d = 1.2f_{spike}$  for model F, so  $f_{max}$  can not be changed with respect to  $f_d$  or  $f_{spike}$ . The simulation procedure is as follows: first,  $4 \times 10^6$  samples of complex, zero-mean white Gaussian noise are generated and filtered; then, the resulting series is interpolated by a factor  $I = 16$  [using *Matlab* function `interp1()` with linear interpolation] resulting in 64 million samples at  $f_s = 4800f_d$ . The interpolated series is then used to compute the complex autocorrelation and other relevant statistics. As is seen, particularly from the inset which details the ACF near  $\tau = 0$ , the dependence of  $R(\tau)$  on  $f_{max}$  is quite weak. This suggests that a larger value of  $f_{max}$  can be adopted with no significant changes on the autocorrelation.

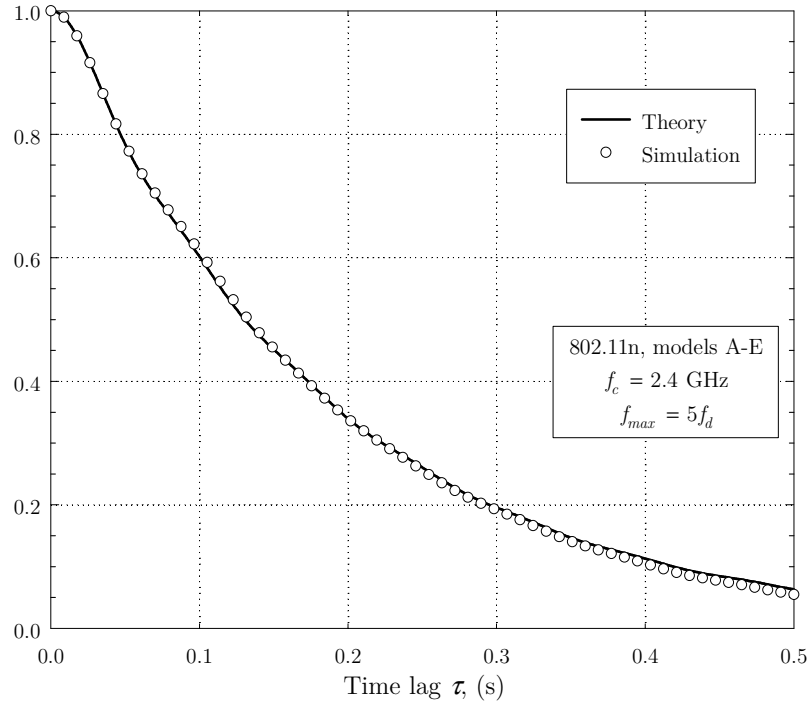


**Figure 2:** Complex autocorrelation  $R(\tau)$  for models A-E (normalized).

For the channel models A-E similar results are presented in Fig. 2 (in this case the PSD has even symmetry and the autocorrelation is real). To compare the performance speedup of (5) over a custom integration routine, we have conducted a simple computational timing comparison of  $R(\tau)$  in *Matlab* using model F parameters with  $f_{max} = 1.2f_{spike}$ . A large number (100000) of uniformly-spaced autocorrelation lags  $0 \leq \tau \leq 2s$  were generated and  $R(\tau)$  was computed from (5) using the function `expint()` for  $E_1(z)$  and from  $R(\tau) = \int_{-f_{max}}^{f_{max}} S(f)e^{j2\pi f\tau} df$  using the numerical (vectorized) integration routine `integral()` with a target absolute error of  $10^{-6}$  and an absolute relative error of  $10^{-3}$ . The speedups observed were approximately 15 and

32 for 802.11ac with  $f_c = 2.4$  GHz and  $f_c = 5.25$  GHz, respectively (21 and 55 for 802.11n). The speedup increases as  $f_d$  and/or  $f_{spike}$  (and therefore  $f_{max}$ ) increases: for example, when the cut-off frequency is increased to  $f_{max} = 5f_{spike}$ , the previous speedups increase to approximately 56, 86, 133 and 195 respectively.

### 3 Level Crossing Rate and Average Fade Duration

The level crossing rate and average fade duration are two important second order statistics for the characterization of the fading process envelope. Given an arbitrary level  $r$ , the LCR is defined as the average frequency that the signal envelope crosses  $r$  with positive slope and the AFD as the average time that the signal envelope remains below  $r$  [9]. For a Rician fading process, these are given by [9, eqs. (16) and (23)], [10]

$$\begin{aligned} \text{LCR}_{\text{Rice}}(\rho) &= \sqrt{\frac{b_2}{b_0} - \left(\frac{b_1}{b_0}\right)^2} \frac{2\sqrt{K+1}}{\pi^{3/2}} \rho e^{-K-(K+1)\rho^2} \cdot \\ &\cdot \int_0^{\pi/2} \cosh\left(2\sqrt{K(K+1)}\rho \cos \theta\right) \left(e^{-\chi^2 \sin^2 \theta} + \sqrt{\pi}\chi \sin \theta \operatorname{erf}(\chi \sin \theta)\right) d\theta \end{aligned} \quad (7)$$

and

$$\text{AFD}_{\text{Rice}}(\rho) = \frac{1 - Q\left(\sqrt{2K}, \sqrt{2(K+1)}\rho\right)}{\text{LCR}_{\text{Rice}}(\rho)} \quad (8)$$

where  $\rho \triangleq \frac{r}{\sqrt{\Omega}}$  is the normalized crossing level;  $\chi \triangleq b_1 \sqrt{\frac{K}{b_0 b_2 - b_1^2}}$ ;  $\operatorname{erf}(\cdot)$  is the error function;  $Q(\cdot, \cdot)$  is the Marcum- $Q$  function and  $b_n$ ,  $n = 0, 1, 2, \dots$  are the spectral moments defined as [9]  $b_n \triangleq \frac{1}{2} \int_{-\infty}^{\infty} (2\pi f)^n S(f) df = \frac{(-j)^n}{2} \frac{\partial^n R(\tau)}{\partial \tau^n} \Big|_{\tau=0}$ . For Rayleigh fading ( $K = 0$ ), these expressions simplify to [9]  $\text{LCR}_{\text{Rayleigh}}(\rho) = \sqrt{\frac{b_2}{b_0} - \left(\frac{b_1}{b_0}\right)^2} \frac{\rho}{\sqrt{\pi}} e^{-\rho^2}$  and  $\text{AFD}_{\text{Rayleigh}}(\rho) = \frac{1 - e^{-\rho^2}}{\text{LCR}_{\text{Rayleigh}}(\rho)}$ . It is worth noting that if  $S(f)$  has even symmetry, as is the case for models A-E, then  $b_1 = 0$ ,  $\chi = 0$  and the LCR simplifies to  $\text{LCR}_{\text{Rice}}(\rho) = \sqrt{\frac{b_2}{b_0} \frac{K+1}{\pi}} \rho e^{-K-(K+1)\rho^2} I_0(2\sqrt{K(K+1)}\rho)$ . However, for channel model F,  $S(f)$  lacks even symmetry,  $b_1 \neq 0$  and (7) must be used. With respect to the 802.11n/ac channel models, the spectral moments  $b_n$  may be computed from the closed expression (5) for  $R(\tau)$  but it is far simpler to compute them from the integral definition given above using  $S(f)$  in (3) and the indefinite integral [11, eq. (2.146-1)]. For the required first three moments the results are

$$b_0 = \frac{1}{2} R(0), \quad (9a)$$

$$b_1 = K_0 f_d \frac{\pi B \xi_0^2}{2C} \left[ 2\sqrt{C} \left( \arctan\left(\sqrt{C}(\xi_s - 1)\right) + \arctan\left(\sqrt{C}(\xi_s + 1)\right) \right) + \log \frac{1 + C(\xi_s - 1)^2}{1 + C(\xi_s + 1)^2} \right] \quad (9b)$$

and

$$b_2 = K_0 f_d^2 2\pi^2 \left[ \frac{2\xi_d}{A} \left( 1 - \frac{\arctan(\sqrt{A}\xi_d)}{\sqrt{A}\xi_d} \right) \right. \quad (9c)$$

$$\left. + \frac{B\xi_0^3}{C} \left( \frac{C-1}{\sqrt{C}} \left( \arctan(\sqrt{C}(\xi_s-1)) + \arctan(\sqrt{C}(\xi_s+1)) \right) + 2\xi_s + \log \frac{1+C(\xi_s-1)^2}{1+C(\xi_s+1)^2} \right) \right]. \quad (9d)$$

To overcome the numerical integration required in (7), the following new series expansion for the LCR of Rician fading envelopes may be used

$$\text{LCR}_{\text{Rice}}(\rho) = \underbrace{\sqrt{\frac{b_2}{b_0} - \left(\frac{b_1}{b_0}\right)^2} \sqrt{\frac{K+1}{\pi}} \rho e^{-K-(K+1)\rho^2} G(\rho, K, \chi)}_{\triangleq H} \quad (10)$$

with

$$G(\rho, K, \chi) \triangleq \begin{cases} I_0(a) + \sum_{n=1}^{\infty} (-1)^{n-1} \underbrace{\frac{\Gamma(n+\frac{1}{2})}{\sqrt{\pi}(2n-1)n!} \left(\frac{2\chi^2}{a}\right)^n}_{\triangleq c_n} I_n(a), & a > 0, \chi \geq 0 \\ 1, & a = 0 \end{cases} \quad (11)$$

where  $a \triangleq 2\sqrt{K(K+1)}\rho$ ;  $\Gamma(\cdot)$  is the gamma function and  $I_n(\cdot)$  is the  $n$ -th-order modified Bessel function. This expansion is derived in Appendix B. The following theorem summarizes some well-known results on the theory of alternating series which will be required in the subsequent analysis.

**Theorem 1.** *Let  $S \triangleq \sum_{n=1}^{\infty} (-1)^{n-1} c_n$  be an alternating series with the  $c_n$  satisfying **i)**  $c_n > 0$  for all  $n$ ; **ii)**  $c_{n+1} < c_n$  for all  $n \geq n_0$  with  $n_0$  some finite integer and **iii)**  $\lim_{n \rightarrow \infty} c_n = 0$ . Also, let  $S_N = \sum_{n=1}^N (-1)^{n-1} c_n$  denote the partial sum of the first  $N$  terms so  $S = \lim_{n \rightarrow \infty} S_N$ . Then, 1) The series is convergent (Leibniz criterion) and  $S > 0$ ; 2) For  $N \geq n_0$  the absolute error (AE) is upper-bounded as  $\varepsilon_A \triangleq |S - S_N| \leq c_{N+1}$ ; 3) For  $N \geq n_0$  the series is bounded as  $S_N < S < S_{N+1}$  if  $N$  is even and  $S_{N+1} < S < S_N$  if  $N$  is odd; 4) For  $N \geq n_0$  the absolute relative error (ARE) is upper-bounded as  $\varepsilon_R \triangleq \frac{|S-S_N|}{S} \leq \frac{c_{N+1}}{S_N}$  if  $N$  is even and  $S_N > 0$ , and  $\varepsilon_R \leq \frac{c_{N+1}}{S_{N+1}} = \frac{c_{N+1}}{S_N - c_{N+1}}$  if  $N$  is odd and  $S_{N+1} > 0$ .*

*Proof.* The proof for parts 1)–3) may be found on many references and textbooks e.g., [12, 13]. For part 4)  $\varepsilon_R \triangleq \frac{|S-S_N|}{S} = \frac{\varepsilon_A}{S}$  and, for  $N \geq n_0$ , it follows from 2) that  $\varepsilon_R \leq \frac{c_{N+1}}{S}$  and from 3)

that  $\varepsilon_R \leq \frac{C_{N+1}}{S_N}$  if  $N$  is even and  $S_N$  positive (because in this case  $S_N < S$ ) or  $\varepsilon_R \leq \frac{C_{N+1}}{S_{N+1}}$  if  $N$  is odd and  $S_{N+1}$  positive (because in this case  $S_{N+1} < S$ ). If  $N$  is odd then  $S_{N+1} = S_N - c_{N+1}$  and the last equality follows.  $\square$

It is interesting to note that the results in this theorem remain valid even when the series only starts alternating for some  $n \geq n_1$ , with  $n_1$  some finite integer [12]. In the following we present a brief characterization of the series  $S$  and use the results in Theorem 1 to obtain limits on the absolute error and absolute relative error (i.e., precision) of the LCR computed from (10) when  $S$  is truncated to a finite number of terms in (11).

**Theorem 2.** *Let  $S$  be the infinite series as defined in (11) with coefficients  $c_n$ . Then 1)  $c_n \geq 0$  for all  $n \geq 1$  meaning that  $S$  is an alternating series with positive first term  $c_1$ ; 2)  $\lim_{n \rightarrow \infty} c_n = 0$ ; 3) A finite integer  $n_0$  exists such that  $c_{n+1} < c_n$  for all  $n \geq n_0 \triangleq \max(1, \lceil \chi^2 - 1 \rceil)$  where  $\lceil \cdot \rceil$  is the ceiling function.*

*Proof.* 1) This follows immediately from the definition of the special functions entering the  $c_n$  expression. 2) The coefficients can be written as the product  $c_n = f_1(n) \cdot f_2(n)$  with  $f_1(n) = \frac{\Gamma(n+\frac{1}{2})}{\sqrt{\pi}(2n-1)\Gamma(n+1)}$  and  $f_2(n) = \left(\frac{2\chi^2}{a}\right)^n I_n(a)$ . Using the asymptotic expansion [11, eq. (8.327)]  $\Gamma(z) \sim \sqrt{2\pi} z^{z-\frac{1}{2}} e^{-z}$ ,  $z \rightarrow \infty$  we may write, after simplification,  $f_1(n) \sim \frac{\sqrt{n+1}}{\sqrt{\pi}(2n-1)(n+\frac{1}{2})} \left(1 - \frac{\frac{1}{2}}{n+1}\right)^{n+1} e^{\frac{1}{2}}$ ,  $n \rightarrow \infty$ . Taking the limit  $n \rightarrow \infty$ , the first factor  $\frac{\sqrt{n+1}}{\sqrt{\pi}(2n-1)(n+\frac{1}{2})}$  goes to zero and  $\left(1 - \frac{\frac{1}{2}}{n+1}\right)^{n+1} e^{\frac{1}{2}} \rightarrow 1$  so  $\lim_{n \rightarrow \infty} f_1(n) = 0$ . As for  $f_2(n)$ , using the asymptotic expansion [14, eq. (10.41.1)]  $I_n(a) \sim \frac{1}{\sqrt{2\pi n}} \left(\frac{ea}{2n}\right)^n$ ,  $n \rightarrow \infty$ ,  $n \gg a$ ,  $f_2(n) \sim \frac{1}{\sqrt{2\pi n}} \left(\frac{e\chi^2}{2n}\right)^n$  independent of  $a$  and  $\lim_{n \rightarrow \infty} f_2(n) = 0$  for any finite  $\chi$ . This shows that  $\lim_{n \rightarrow \infty} c_n = 0$  for all  $a$  and  $\chi$ . 3) We have to prove that  $\frac{c_{n+1}}{c_n} < 1$  for all  $n \geq n_0$ . The coefficient ratio is written as

$$\frac{c_{n+1}}{c_n} = \frac{(2n-1)\Gamma(n+1)\Gamma\left(n+\frac{3}{2}\right)}{(2n+1)\Gamma(n+2)\Gamma\left(n+\frac{1}{2}\right)} \left(\frac{2\chi^2}{a}\right) \frac{I_{n+1}(a)}{I_n(a)}. \quad (12)$$

For the first factor we may write, using [11, eq. (8.339-2)]

$$\begin{aligned} \frac{(2n-1)\Gamma(n+1)\Gamma\left(n+\frac{3}{2}\right)}{(2n+1)\Gamma(n+2)\Gamma\left(n+\frac{1}{2}\right)} &= \frac{(2n-1)\frac{\sqrt{\pi}}{2^{n+1}}(2n+1)!!}{(2n+1)(n+1)\frac{\sqrt{\pi}}{2^n}(2n-1)!!} = \frac{(2n-1)(2n+1)!!}{2(n+1)\underbrace{(2n+1)(2n-1)!!}_{(2n+1)!!}} \\ &= \frac{2n-1}{2n+2} < 1, \quad n \geq 1. \end{aligned} \quad (13)$$

From the identity  $zI_{n-1}(z) - zI_{n+1}(z) = 2nI_n(z)$  [11, eq. (8.486-1)] we have  $\frac{2}{z} \frac{I_{n+1}(a)}{I_n(a)} = \frac{1}{n+1} \left(1 - \frac{I_{n+2}(a)}{I_n(a)}\right)$  and thus, for the product of the two last factors in (12)

$$\left(\frac{2\chi^2}{a}\right) \frac{I_{n+1}(a)}{I_n(a)} = \frac{\chi^2}{n+1} \left(1 - \frac{I_{n+2}(a)}{I_n(a)}\right) \leq \frac{\chi^2}{n+1} \quad (14)$$

because  $0 \leq \frac{I_{n+2}(a)}{I_n(a)} < 1$  for all  $a > 0$  which follows from  $I_n(a)$  being strictly decreasing as  $n$  increases, with fixed  $a$  [14, Sec. 10.37]. The left equality is attained for  $a = 0$ . Therefore  $\frac{\chi^2}{n+1} < 1$  requires  $n > \lceil \chi^2 - 1 \rceil$ . For small values of  $\chi$  this may give values less than 1, meaning that any  $n \geq 1$  suffices, so  $n \geq n_0 \triangleq \max(1, \lceil \chi^2 - 1 \rceil)$ . We note that, due to the use of several upper bounds on this derivation,  $n_0$  is not necessarily the *minimum* value of  $n$  for which  $\frac{c_{n+1}}{c_n} < 1$  but it is guaranteed that if  $n \geq n_0$  then  $\frac{c_{n+1}}{c_n} < 1$ .  $\square$

### 3.1 LCR error characterization

We will now apply Theorem 1 to characterize the LCR expression (10). For the series  $S$  in (11) the partial sums  $S_N$  are

$$S_N \triangleq \sum_{n=1}^N (-1)^{n-1} \frac{\Gamma(n + \frac{1}{2})}{\sqrt{\pi}(2n-1)n!} \left(\frac{2\chi^2}{a}\right)^n I_n(a). \quad (15)$$

Taking into account the results in Theorem 2 we may conclude that the series  $S$  is convergent for all values of  $a \geq 0$  and  $\chi \geq 0$ . In addition, recalling from (10) and (11) that the LCR is [the factor  $H > 0$  is defined in (10)]

$$\text{LCR}_{\text{Rice}}(\rho) = H \cdot (I_0(a) + S) \quad (16)$$

the absolute error in the computation of the LCR using  $N$  terms for  $S$  is upper bounded by

$$\varepsilon_A(\text{LCR}) = |H \cdot (I_0(a) + S) - H \cdot (I_0(a) + S_N)| = H \cdot |S - S_N| = H\varepsilon_A \leq H \cdot c_{N+1}, \quad N \geq n_0 \quad (17)$$

and the absolute relative error by

$$\begin{aligned} \varepsilon_R(\text{LCR}) &= \frac{\varepsilon_A(\text{LCR})}{\text{LCR}_{\text{Rice}}(\rho)} = \frac{\varepsilon_A(\text{LCR})}{H \cdot (I_0(a) + S)} \leq \frac{c_{N+1}}{I_0(a) + S} \\ &\leq \begin{cases} \frac{c_{N+1}}{I_0(a) + S_N}, & N \geq n_0, N \text{ even}, I_0(a) + S_N > 0 \\ \frac{c_{N+1}}{I_0(a) + S_N - c_{N+1}}, & N \geq n_0, N \text{ odd}, I_0(a) + S_N - c_{N+1} > 0 \end{cases}. \end{aligned} \quad (18)$$

Noting that  $c_{N+1} > 0$  we may also use, for  $N$  even, the slightly looser upper bound stated in (18) for  $N$  odd, so finally

$$\varepsilon_R(\text{LCR}) \leq \frac{c_{N+1}}{I_0(a) + S_N - c_{N+1}}, \quad N \geq n_0, \quad I_0(a) + S_N > c_{N+1}. \quad (19)$$

The result (19) is quite useful in practice since it may be used to monitor the ARE as the computation progresses and provide a stopping criterion for the computation. For example if an LCR result with  $P$  decimal digits accuracy is desired, the value of  $N$  needs only be increased

until  $\varepsilon_R(\text{LCR}) < 10^{-P}$ . It should be noted that the constraint involving  $S_N$  in (19) [or in part 4) of theorem (2) for that matter] is not restrictive at all since it will be verified as  $N$  increases because  $I_0(a) + \frac{1}{\sqrt{\pi}}S_N$  is the LCR estimate computed with  $N$  terms, which will approach a positive value (i.e., the true LCR, equal to  $I_0(a) + \frac{1}{\sqrt{\pi}}S$ ) and, as proved before,  $c_{N+1} \rightarrow 0$  as  $N$  increases. As for the condition  $N \geq n_0$  it is also not restrictive since it will always be satisfied if a reasonable small value for the target ARE is specified. The following *Matlab* script illustrates the computation of the LCR with a prescribe precision of  $P$  decimal digits.

MATLAB SCRIPT TO COMPUTE THE LCR USING (10) AND (19)

```
function lcr=LCR_Series(H,a,chi,P);
% H = H, a = a, chi = χ, P = target precision (decimal digits)
SR_PI=sqrt(pi);           % √π
are_target=10^(-P);       % target precision
lcr=besseli(0,a);          % first term
n=1;
c=gamma(n+1/2)/(SQRT_PI*(2*n-1)*gamma(n+1))*(2*chi^2/a)^n*besseli(n,a); % c1
are_actual=1;              % current precision
while are_actual > are_target
    lcr=lcr+(-1)^(n-1)*c;   % update Sn = Sn-1 + (-1)n-1cn
    n=n+1;
    c=gamma(n+1/2)/(SR_PI*(2*n-1)*gamma(n+1))*(2*chi^2/a)^n*besseli(n,a); % cn+1
    are_actual=c/(lcr-c);   % ARE =  $\frac{c_{n+1}}{S_n - c_{n+1}}$ 
end
lcr=H*lcr;                 % compute final value of the LCR
```

### Notational remark

The notation used in the previous Section was adopted to facilitate the analysis but, because the first term  $I_0(a)$  is not included in the sum over  $n$ , does not lead to the simplest expressions for the absolute relative error. For a more clear, compact ARE expression, we may redefine  $G(\rho, K, \chi)$  as

$$G(\rho, K, \chi) \triangleq \begin{cases} \overbrace{\sum_{n=0}^{\infty} (-1)^{n-1} \frac{\Gamma(n + \frac{1}{2})}{\sqrt{\pi}(2n-1)n!} \left(\frac{2\chi^2}{a}\right)^n I_n(a)}^{\triangleq S} & a > 0, \chi > 0 \\ I_0(a), & \chi = 0 \\ 1, & a = 0 \end{cases} \quad (20)$$

so with  $S_N \triangleq \sum_{n=0}^N (-1)^{n-1} c_n$ , (19) becomes

$$\varepsilon_R(\text{LCR}) \leq \frac{c_{N+1}}{S_N - c_{N+1}}, \quad N \geq n_0, \quad S_N > c_{N+1}. \quad (21)$$

It must be noted that now  $S_N$  involves the summation of the first  $N + 1$  terms of the series.



### 3.2 AFD error characterization

Let us consider two functions  $f$  and  $g$  related by  $g = \frac{D}{f}$  with  $D$  some constant and an estimate of  $f$ ,  $\hat{f}$  obtained by some numerical method with an ARE  $\varepsilon_f \triangleq \left| \frac{f - \hat{f}}{\hat{f}} \right|$ . We take an estimate of  $g$  as  $\hat{g} = \frac{K}{\hat{f}}$ . The absolute relative error of  $g$  is then

$$\varepsilon_g \triangleq \left| \frac{g - \hat{g}}{g} \right| = \left| \frac{\frac{D}{f} - \frac{D}{\hat{f}}}{\frac{D}{f}} \right| = \left| \frac{\hat{f} - f}{\hat{f}} \right| = \left| \frac{\hat{f} - f}{f} \right| \cdot \left| \frac{f}{\hat{f}} \right| = \varepsilon_f \left| \frac{f}{\hat{f}} \right|. \quad (22)$$

If  $\hat{f} > f$  then  $\frac{f}{\hat{f}} = 1 - \varepsilon_f$ . If  $\hat{f} < f$  then  $\frac{f}{\hat{f}} = 1 + \varepsilon_f$ . In either case, for reasonably small values of  $\varepsilon_f$ ,  $\left| \frac{f}{\hat{f}} \right| \approx 1$ , meaning that  $\varepsilon_g \approx \varepsilon_f$ . From (8) we see that the relation between  $\text{AFD}_{\text{Rice}}(\rho)$  and  $\text{LCR}_{\text{Rice}}(\rho)$  is the same as that between  $g$  and  $f$  because  $D = 1 - Q\left(\sqrt{2K}, \sqrt{2(K+1)}\rho\right)$  is constant in this context. Therefore, the ARE for the computation of the  $\text{AFD}_{\text{Rice}}(\rho)$  may be taken as approximately the same obtained from (19) for the  $\text{LCR}_{\text{Rice}}(\rho)$ .

### 3.3 Results and discussion

In this Section, several numerical results pertaining to the LCR and AFD using the proposed computational expressions are presented. The ARE for the computation of the LCR from (10) using (15) with  $N = 5$  terms is shown in Fig. 3 as a function of  $\rho$  and  $K$  using the  $b_n$  pertaining to the 802.11n channel model  $F$  with  $f_c = 2.4$  GHz. The true value of the LCR was also computed from (15) using  $N = 120$  terms. For fixed  $K$ , the ARE decreases as  $\rho$  increases and for fixed  $\rho$  decreases as  $K$  decreases. We have verified that for different values of the moments  $b_n$ , which impact the value of  $\chi$ , the behaviour is similar and particularly so for 802.11n/ac with either carrier frequency. Another useful application of the upper bound (19) is to determine the number of terms required in (15) to achieve some target precision in the computation of the LCR. Fig. 4 illustrates such a result, for a target precision of  $P = 5$  decimal digits precision [i.e.  $\varepsilon_R(\text{LCR}) \leq 10^{-5}$ ], as a function of  $K$  and  $\rho$  for the 802.11n channel model  $F$ . As is seen, even for the wide range of  $k$  and  $\rho$  considered, the number of terms is small. Fig. 5 shows the true number of terms required. As might have been anticipated in view of the upper bound nature of the result, for some values of  $K$  and  $\rho$  the values of  $N$  in Fig. 4 are higher than those actually needed (Fig. 5). The difference, however, is small.

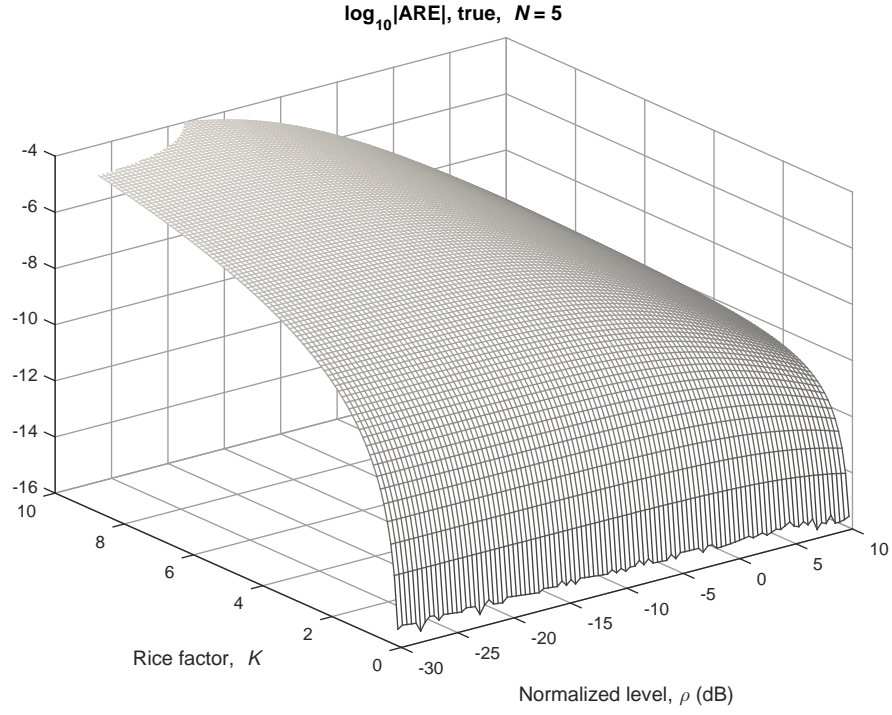


**Figure 3:** True absolute relative error for the LCR computed from (10) using (15) with  $N = 5$  terms for the 802.11n standard channel model F with  $f_c = 2.4$  GHz.

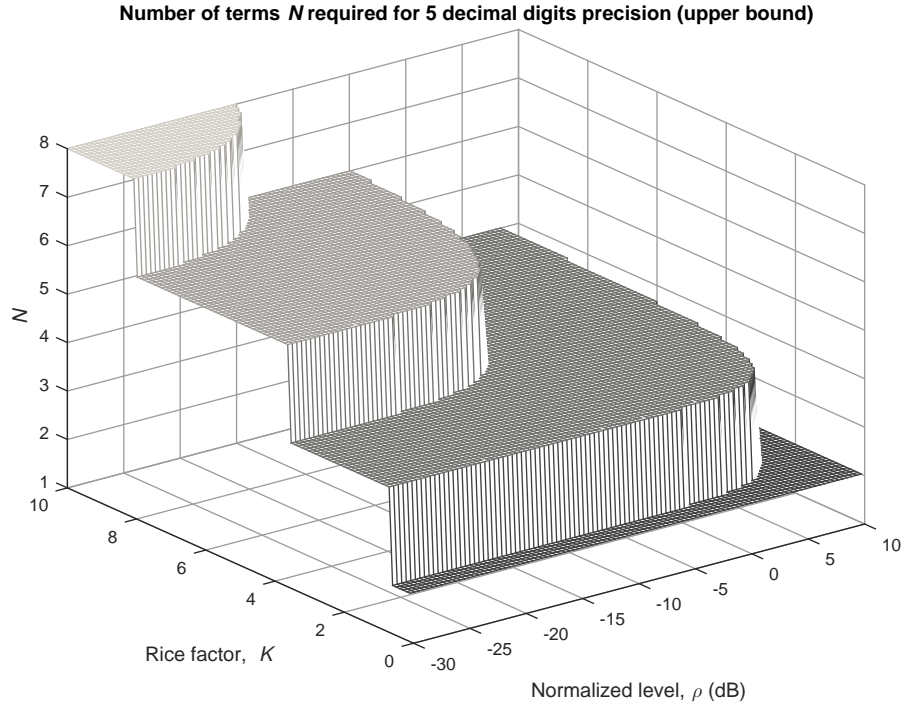


**Figure 4:** Upper bound on the number of terms  $N$  required in (15) to achieve an ARE of  $10^{-5}$ , obtained from (19), for the 802.11n standard channel model F with  $f_c = 2.4$  GHz.

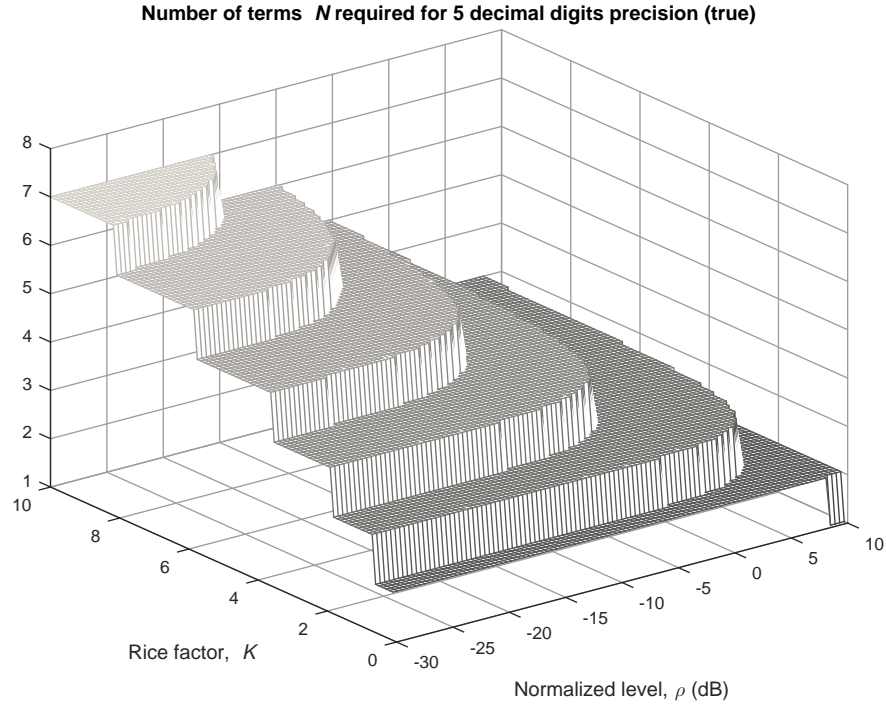


**Figure 5:** True number of terms  $N$  required in (15) to achieve an ARE of  $10^{-5}$  for the 802.11n standard channel model F with  $f_c = 2.4$  GHz.

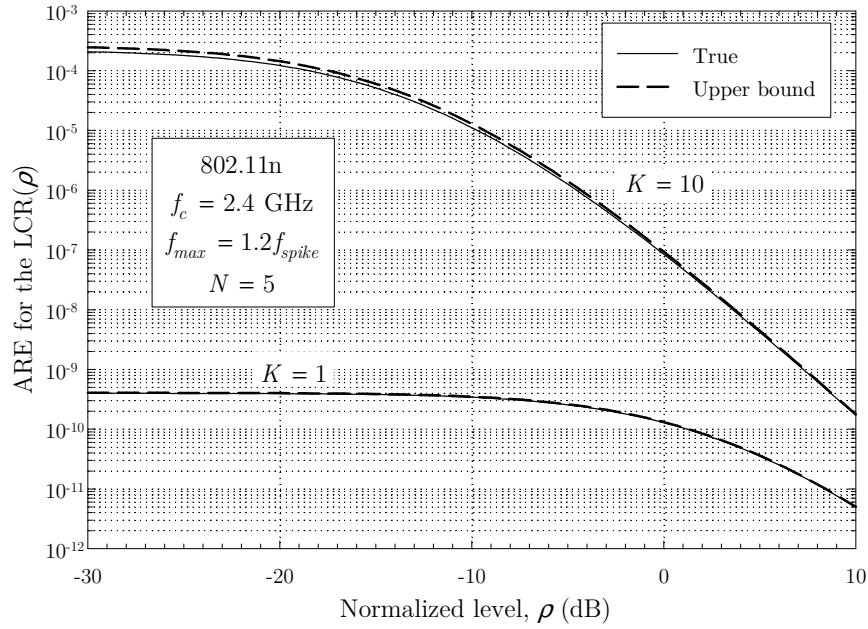


**Figure 6:** Absolute relative error for the LCR as a function of the level  $\rho$ .

Figs. 6 and 7 plot the true value of the ARE (the true value of the LCR was computed using  $N = 120$  terms) and the upper bound (19) as a function of  $\rho$  and  $K$  respectively, for  $N = 5$ . The purpose of these two figures is to show that (19) is quite tight even for the wide range of  $K$  and  $\rho$  considered.

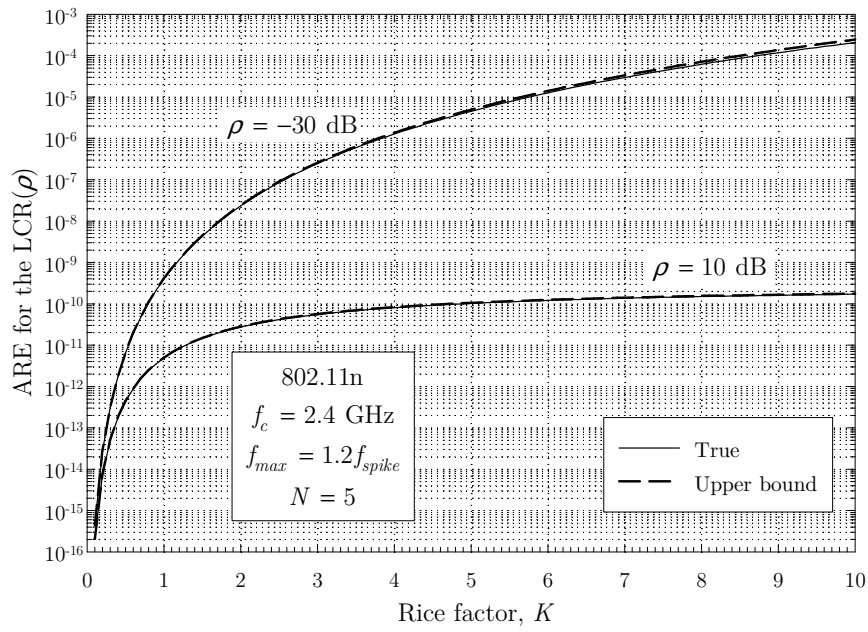


**Figure 7:** Absolute relative error for the LCR as a function of the Rice factor  $K$ .

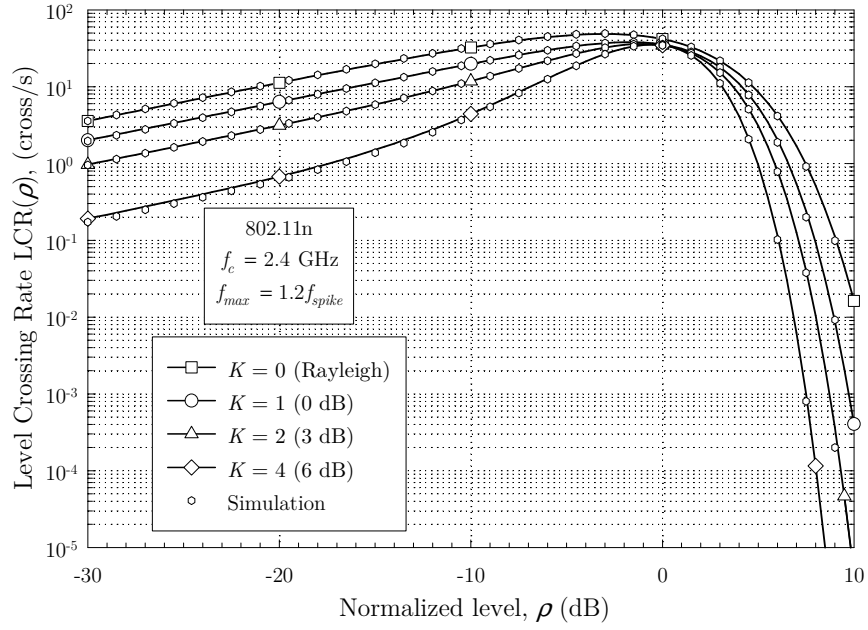


**Figure 8:** Level crossing rate for the 802.11n standard channel model F with  $f_c = 2.4$  GHz.

The LCR and the AFD are represented in Figs. 8 and 9, respectively, as a function of the normalized level  $\rho$ , for different values of the Rice factor  $K$ . These results were computed from (10) and (8) with  $f_{max} = 1.2f_{spike}$ . It is seen that the curves exhibit the usual behavior and in particular, the plots converge around  $\rho = 0$  dB, almost independently of the value of  $K$ .

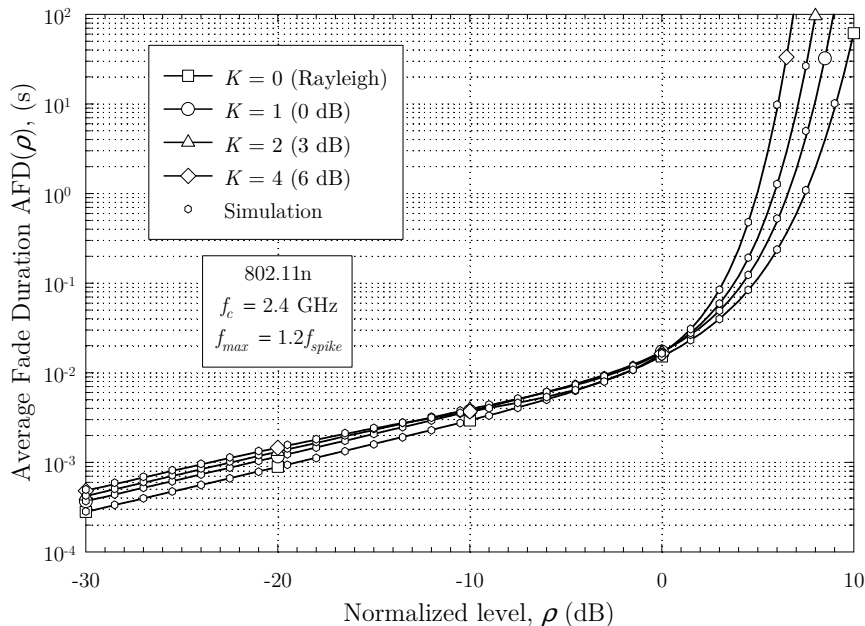


**Figure 9:** Average fade duration for the 802.11n standard channel model F with  $f_c = 2.4$  GHz.

The dependence of the LCR and the AFD on  $f_{max}$  can be inferred from the results in Figs. 10 and 11, which plot these statistics as a function of the ratio  $f_{max}/f_{spike}$  for  $K = 0$  and  $1.2 \leq f_{max}/f_{spike} \leq 10^4$ . It is interesting to note that for  $f_{max}/f_{spike} \lesssim 10$ , the dependence of the LCR and the AFD on this ratio is quite weak but becomes stronger as it increases, eventually leading to LCR and AFD values, which differ significantly from those with small  $f_{max}/f_{spike}$ . Also, we have verified that this weak dependence on  $f_{max}/f_{spike}$  is almost unaffected by  $K$ . Based on this behaviour and recalling that the effect of this ratio on the autocorrelation is also weak, we conclude that in practice a larger value of this ratio, for example  $f_{max}/f_{spike} = 5$  (indicated in Figs. 10 and 11 as a vertical dashed line) may be used. The use of a larger cut-off frequency  $f_{max}$  has the advantage of easing the implementation of practical simulators, since a larger  $f_{max}$  allows the PSD to decay more significantly before being abruptly cut-off at  $f = f_{max}$ . For example, an increase from  $f_{max} = 1.2f_{spike}$  to  $f_{max} = 5f_{spike}$  allows  $S(f)$  in (3) to decrease an additional 16.8 dB for positive frequencies (12.3 dB for negative frequencies) before reaching the cut-off frequency. It is important to note that the use of a finite  $f_{max}$  is mandatory since as  $f_{max} \rightarrow \infty$ ,  $b_2 \rightarrow \infty$  and thus  $LCR \rightarrow \infty$  and  $AFD \rightarrow 0$ . As for the channel models A-E, it can be seen from the results in Fig. 12 that the (real-valued) autocorrelation dependence on  $f_{max}$ , or equivalently on the ratio  $f_{max}/f_d$ , is also quite weak. However, the dependence of the LCR (and the AFD) on this parameter is weak only for small ratios  $f_{max}/f_d \lesssim 0.4$ . A value larger than  $f_{max}/f_d = 5$  (recommended in [1]) may be used to ease the simulator implementation, but it will inevitably lead to a higher LCR and lower AFD.

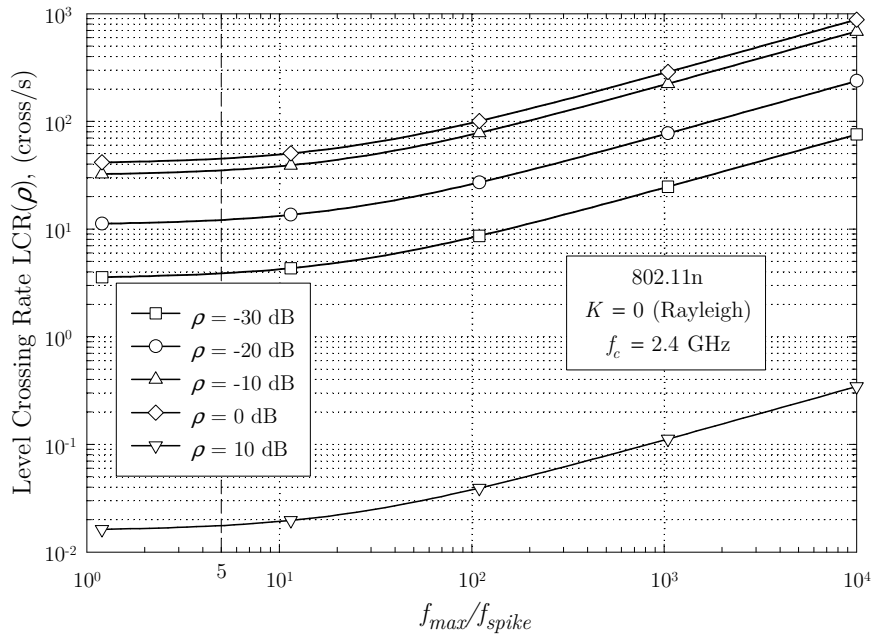


**Figure 10:** Level crossing rate for the 802.11n standard channel model F with  $f_c = 2.4$  GHz as a function of  $f_{max}/f_{spike}$ .

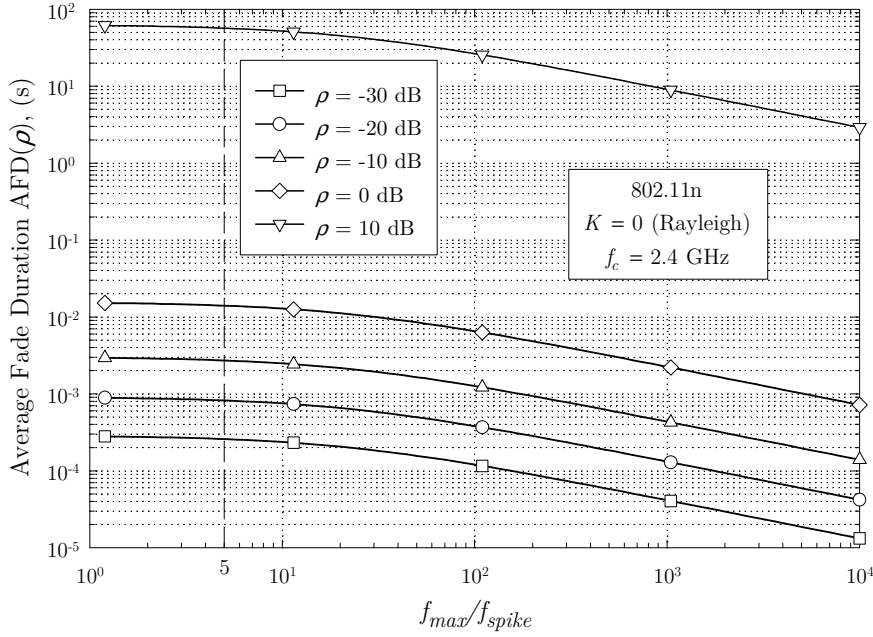


**Figure 11:** Average fade duration for the 802.11n standard channel model F with  $f_c = 2.4$  GHz as a function of  $f_{max}/f_{spike}$ .

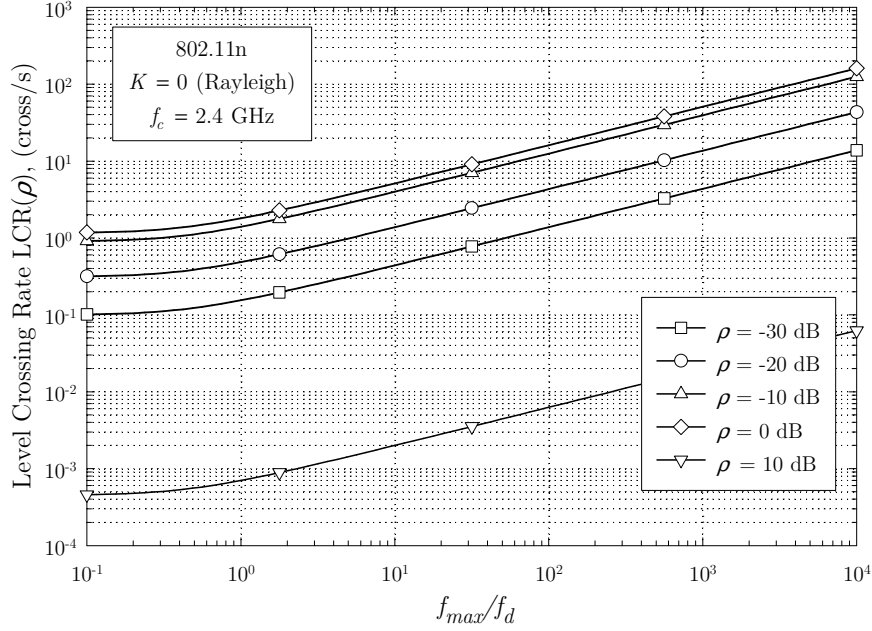


**Figure 12:** Level crossing rate for the 802.11n standard channel models A-E with  $f_c = 2.4$  GHz as a function of  $f_{max}/f_d$ .

## 4 Conclusions

In this report, we have presented closed-form expressions for the complex autocorrelation function and for the spectral moments required to compute the LCR and AFD of the channel models specified in the IEEE 802.11n/ac standard. A series expansion for the LCR (and for the AFD) of Rician fading envelopes and an useful upper bound on the attainable precision of the truncated series were also reported. These expressions overcome the need for custom numerical integration and, although requiring the computation of  $E_1(z)$  and  $I_n(x)$ , may actually benefit from the efficiency and precision of implementations of these special functions, readily available in most mathematical software packages and scientific libraries. These results were used to study the dependence of the autocorrelation, LCR and AFD on the Doppler spectrum cut-off frequency  $f_{max}$  and to conclude that  $f_{max}$  may be increased to facilitate the implementation of practical 802.11n/ac channel simulators without significant changes in the autocorrelation for all the six channel models, or in the LCR and AFD in the case of channel model F.





# Appendix A – Derivation of $I(\tau, \alpha, \beta, \gamma)$ in closed-form

In this Appendix we derive a closed form expression for the integral  $I(\tau, \alpha, \beta, \gamma)$  defined as

$$I(\tau, \alpha, \beta, \gamma) \triangleq \int_{-f_{max}}^{f_{max}} \frac{e^{j2\pi f\tau}}{1 + \alpha \left( \frac{f-\beta}{\gamma} \right)^2} df. \quad (\text{A.1})$$

We consider the restrictions  $\alpha, \gamma > 0$ . Also, because  $I(-\tau, \alpha, \beta, \gamma) = I^*(\tau, \alpha, \beta, \gamma)$ , only  $\tau > 0$  is considered. The case  $\tau = 0$  is addressed separately. The derivation is divided in two cases, depending on the relation between  $f_{max}$  and  $\beta$ .

## A.1 Analysis for $f_{max} > \beta \geq 0$

In terms of the analysis required for 802.11n/ac, one has always  $f_m > \beta$  i.e.,  $f_{max} > f_{spike}$ , the cut-off frequency is always greater than the spike frequency. Factoring the integrand denominator and changing the integration limits, (A.1) may be written as

$$I(\tau, \alpha, \beta, \gamma) = \underbrace{\int_{-\infty}^{\infty} \frac{e^{j2\pi f\tau}}{1 + \alpha \left( \frac{f-\beta}{\gamma} \right)^2} df}_{I_A(\tau, \alpha, \beta, \gamma)} - \frac{\gamma^2}{\alpha} \left( \underbrace{\int_{f_{max}}^{\infty} \frac{e^{j2\pi f\tau}}{(f - z_1)(f - z_1^*)} df}_{I_B(\tau, \alpha, \beta, \gamma)} + \underbrace{\int_{-\infty}^{-f_{max}} \frac{e^{j2\pi f\tau}}{(f - z_1)(f - z_1^*)} df}_{I_C(\tau, \alpha, \beta, \gamma)} \right) \quad (\text{A.2})$$

where  $z_1 \triangleq \beta + j\frac{\gamma}{\sqrt{\alpha}}$ . The three integrals in this expression are now computed individually as follows:

$I_A(\tau, \alpha, \beta, \gamma)$  Making the change of variable  $t = f - \beta$  we have

$$\begin{aligned} I_A(\tau, \alpha, \beta, \gamma) &= e^{j2\pi\beta\tau} \int_{-\infty}^{\infty} \frac{e^{j2\pi t\tau}}{1 + \alpha \left( \frac{t}{\gamma} \right)^2} dt = 2 e^{j2\pi\beta\tau} \int_0^{\infty} \frac{\cos(2\pi t\tau)}{1 + \alpha \left( \frac{t}{\gamma} \right)^2} dt \\ &= e^{j2\pi\beta\tau} \frac{\pi\gamma}{\sqrt{\alpha}} e^{-2\pi\frac{\gamma}{\sqrt{\alpha}}|\tau|} \end{aligned} \quad (\text{A.3})$$

where the last equality follows from the known definite integral [11, eq.(3.723-2)].

$I_B(\tau, \alpha, \beta, \gamma)$  Expanding the integrand in partial fractions we have that

$$\begin{aligned} I_B(\tau, \alpha, \beta, \gamma) &= \frac{\sqrt{\alpha}}{2\gamma j} \left( \int_{f_{max}}^{\infty} \frac{e^{j2\pi f\tau}}{f - z_1} df - \int_{f_{max}}^{\infty} \frac{e^{j2\pi f\tau}}{f - z_1^*} df \right) \\ &= \frac{\sqrt{\alpha}}{2\gamma j} \left( e^{j2\pi z_1\tau} \underbrace{\int_{z_2}^{-j\infty + \Re\{z_2\}} \frac{e^{-t}}{t} dt}_{I_{B1}(\tau, \alpha, \beta, \gamma)} - e^{j2\pi z_1^*\tau} \underbrace{\int_{z_3}^{-j\infty + \Re\{z_3\}} \frac{e^{-t}}{t} dt}_{I_{B2}(\tau, \alpha, \beta, \gamma)} \right) \end{aligned} \quad (\text{A.4})$$

where now  $z_2 \triangleq -j2\pi\tau(f_{max} - z_1) = -2\pi\tau\left(\frac{\gamma}{\sqrt{\alpha}} + j(f_{max} - \beta)\right)$  and  $z_3 \triangleq -j2\pi\tau(f_{max} - z_1^*) = -2\pi\tau\left(-\frac{\gamma}{\sqrt{\alpha}} + j(f_{max} - \beta)\right)$ . To obtain the second equality in (A.4) we performed the change of variable  $t = -j2\pi\tau(f - z_1)$  in the first integral and  $t = -j2\pi\tau(f - z_1^*)$  in the second.

We now digress briefly and consider the exponential integral function defined by the complex integral  $E_1(z) \triangleq \int_z^\infty \frac{e^{-t}}{t} dt, |\arg\{z\}| < \pi, z \neq 0 + j0$  [6, eq (5.1.1)]. It must be noted that  $E_1(z)$  is a multivalued function and that this definition of  $E_1(z)$  is for the principal branch  $|\arg\{z\}| < \pi$ , with a branch cut in the negative real axis [15, p. 31]. Each time the integration path crosses the pole at  $u = 0$ , a contribution of  $\pm j2\pi$  residue  $\left\{\frac{e^{-u}}{u}\right\}_{u=0}$  is made to the integral [p. 1463] [16], the plus (minus) sign being taken if the path is in the clockwise (counterclockwise) direction. Since the residue equals 1, by analytic continuation  $E_1(e^{j2\pi k}) = E_1(z) - j2\pi k$  with  $k$  any integer [16, eq. (2.4)] [14, eq. (6.4.2)].

As can be inferred from their definition in (A.4), the integrals  $I_{B_{1,2}}(\tau, \alpha, \beta, \gamma)$  are closely related to  $E_1(z)$ . Consider the integral  $I_{B_1}(\tau, \alpha, \beta, \gamma)$  which is a multivalued function of  $z_2$ . The path of integration is a vertical line with real part equal to  $\Re\{z_2\}$  and imaginary part ranging from  $\Im\{z_2\}$  down to  $-\infty$ , therefore clockwise oriented. If  $\Im\{z_2\} < 0$  the path does not cross the origin but if  $\Im\{z_2\} \geq 0$  it does and, in lieu of the previous discussion,  $j2\pi$  must be added to the result. In other words, we have

$$\int_{z_2}^{-j\infty + \Re\{z_2\}} \frac{e^{-t}}{t} dt = \begin{cases} E_1(z_2) + j2\pi, & \Im\{z_2\} \geq 0 \\ E_1(z_2), & \Im\{z_2\} < 0 \end{cases}. \quad (\text{A.5})$$

Since  $\tau > 0$  and  $f_{max} > \beta$ , it follows that  $\Im\{z_2\} = \Im\{z_3\} = -2\pi\tau(f_{max} - \beta) < 0$  and thus

$$I_{B_1}(\tau, \alpha, \beta, \gamma) = E_1(z_2) = E_1\left(-2\pi\tau\left(\frac{\gamma}{\sqrt{\alpha}} + j(f_{max} - \beta)\right)\right) \quad (\text{A.6a})$$

and

$$I_{B_2}(\tau, \alpha, \beta, \gamma) = E_1(z_3) = E_1\left(2\pi\tau\left(\frac{\gamma}{\sqrt{\alpha}} - j(f_{max} - \beta)\right)\right) \quad (\text{A.6b})$$

so finally, from (A.4)

$$\begin{aligned} I_B(\tau, \alpha, \beta, \gamma) &= \frac{\sqrt{\alpha}}{2\gamma j} e^{j2\pi\beta\tau} \left( e^{-2\pi\frac{\gamma}{\sqrt{\alpha}}\tau} E_1(-2\pi z_- \tau) - e^{2\pi\frac{\gamma}{\sqrt{\alpha}}\tau} E_1(2\pi z_-^* \tau) \right) \\ &= -\frac{\sqrt{\alpha}}{2\gamma} e^{j2\pi\beta\tau} \left( F(-z_- \tau) - F(z_-^* \tau) \right) \end{aligned} \quad (\text{A.7})$$

where  $z_- \triangleq \frac{\gamma}{\sqrt{\alpha}} + j(f_{max} - \beta)$  and the function  $F(u) \triangleq j e^{2\pi\Re\{u\}} E_1(2\pi u)$  have been defined.

$I_C(\tau, \alpha, \beta, \gamma)$  This integral can be evaluated following the same steps as with  $I_B(\tau, \alpha, \beta, \gamma)$ .

However it is much simpler to note that

$$I_C(\tau, \alpha, \beta, \gamma) = \int_{-\infty}^{-f_{max}} \frac{e^{j2\pi f\tau}}{(f - z_1)(f - z_1^*)} df \stackrel{f \leftarrow -f}{=} \int_{f_{max}}^{\infty} \frac{e^{-j2\pi f\tau}}{(f + z_1)(f + z_1^*)} df \quad (\text{A.8})$$

so, from (A.2) we may obtain  $I_C(\tau, \alpha, \beta, \gamma)$  by setting  $\tau \leftarrow -\tau$  and  $z_1 \leftarrow -z_1$  in (A.7), or equivalently  $I_C(\tau, \alpha, \beta, \gamma) = I_B(-\tau, \alpha, -\beta, -\gamma) = I_B(-\tau, -\alpha, -\beta, \gamma)$ . The result is

$$\begin{aligned} I_C(\tau, \alpha, \beta, \gamma) &= -\frac{\sqrt{\alpha}}{2\gamma j} e^{j2\pi\beta\tau} \left( e^{-2\pi\frac{\gamma}{\sqrt{\alpha}}\tau} E_1(-2\pi z_+^* \tau) - e^{2\pi\frac{\gamma}{\sqrt{\alpha}}\tau} E_1(2\pi z_+ \tau) \right) \\ &= \frac{\sqrt{\alpha}}{2\gamma} e^{j2\pi\beta\tau} \left( F(-z_+^* \tau) - F(z_+ \tau) \right) \end{aligned} \quad (\text{A.9})$$

where  $z_+ \triangleq \frac{\gamma}{\sqrt{\alpha}} + j(f_{max} + \beta)$  has been defined.

At this point we are able to return to (A.2) and, using (A.7) and (A.9), write the final result for  $\tau > 0$  as

$$\begin{aligned} I(\tau, \alpha, \beta, \gamma) &= I_A(\tau, \alpha, \beta, \gamma) - \frac{\gamma^2}{\alpha} (I_B(\tau, \alpha, \beta, \gamma) + I_C(\tau, \alpha, \beta, \gamma)) = e^{j2\pi\beta\tau} \frac{\pi\gamma}{\sqrt{\alpha}} e^{-2\pi\frac{\gamma}{\sqrt{\alpha}}|\tau|} \\ &\quad - \frac{\gamma^2}{\alpha} \left( -\frac{\sqrt{\alpha}}{2\gamma} e^{j2\pi\beta\tau} \left( F(-z_- \tau) - F(z_-^* \tau) \right) + \frac{\sqrt{\alpha}}{2\gamma} e^{j2\pi\beta\tau} \left( F(-z_+^* \tau) - F(z_+ \tau) \right) \right) \\ &= \frac{\gamma}{2\sqrt{\alpha}} e^{j2\pi\beta\tau} \left[ 2\pi e^{-2\pi\frac{\gamma}{\sqrt{\alpha}}|\tau|} + F(-z_- \tau) - F(z_-^* \tau) - F(-z_+^* \tau) + F(z_+ \tau) \right]. \end{aligned} \quad (\text{A.10})$$

For  $\tau = 0$ ,  $z_{\pm} = 0$  and the functions  $E_1(0)$  and  $F(0)$  are undefined. However, from (A.1)

$$\begin{aligned} I(0, \alpha, \beta, \gamma) &= \int_{-f_{max}}^{f_{max}} \frac{1}{1 + \alpha \left( \frac{f - \beta}{\gamma} \right)^2} df \\ &= \frac{\gamma}{\sqrt{\alpha}} \left[ \arctan \left( \sqrt{\alpha} \frac{f_{max} - \beta}{\gamma} \right) + \arctan \left( \sqrt{\alpha} \frac{f_{max} + \beta}{\gamma} \right) \right] \end{aligned} \quad (\text{A.11})$$

which has been obtained from the known definite integral [11, eq. (2.124-1)]. Finally, combining (A.10) and (A.11) gives (4) in the main text, as we intended to prove.

In the 802.11n/ac channel models A-E vehicle movement is absent. To reflect this fact in the previous autocorrelation results, we have to consider  $f_{spike} = 0$ , or equivalently  $\beta = 0$ . In this case,  $z_- = z_+ = \frac{\gamma}{\sqrt{\alpha}} + jf_{max} \triangleq z_0$ . From its definition and the fact that  $E_1^*(z) = E_1(z^*)$ , we have  $F^*(u) = -F(u^*)$  and from (A.10)

$$\begin{aligned} I(\tau, \alpha, 0, \gamma) &= \frac{\gamma}{2\sqrt{\alpha}} \left[ 2\pi e^{-2\pi\frac{\gamma}{\sqrt{\alpha}}|\tau|} + F(-z_0\tau) - F(z_0^*\tau) - F(-z_0^*\tau) + F(z_0\tau) \right] \\ &= \frac{\gamma}{2\sqrt{\alpha}} \left[ 2\pi e^{-2\pi\frac{\gamma}{\sqrt{\alpha}}|\tau|} + F(-z_0\tau) + F^*(z_0\tau) + F^*(-z_0\tau) + F(z_0\tau) \right] \\ &= \frac{\gamma}{\sqrt{\alpha}} \left[ \pi e^{-2\pi\frac{\gamma}{\sqrt{\alpha}}|\tau|} + \Re \{ F(-z_0\tau) + F(z_0\tau) \} \right] \end{aligned} \quad (\text{A.12})$$

which justifies the first term in the second equality in (5). Also, from (A.11),  $I(0, \alpha, 0, \gamma) = \frac{2\gamma}{\sqrt{\alpha}} \arctan\left(\sqrt{\alpha} \frac{f_{max}}{\gamma}\right)$  which justifies the first term in the right-hand side of (6).

## A.2 Analysis for $0 < f_{max} \leq \beta$

As stated previously, the results presented above are sufficient analysis required for the analysis of 802.11n/ac autocorrelation because one has always  $f_m > \beta$  i.e.,  $f_{max} > f_{spike}$ . It is nevertheless interesting to make use of the previous analysis and address also the case  $0 < f_{max} \leq \beta$ . The results for  $I_A(\tau, \alpha, \beta, \gamma)$  are the same. When  $\tau > 0$ ,  $\Im\{z_2\} = -2\pi\tau(f_m - \beta) \geq 0$  but  $\Im\{z_3\} = -2\pi\tau(f_m + \beta) < 0$ . In lieu of (A.5), this means that  $j2\pi$  must be added to  $I_{B_1}(\tau, \alpha, \beta, \gamma)$  but not to  $I_{B_2}(\tau, \alpha, \beta, \gamma)$ , so

$$\begin{aligned} I_B(\tau, \alpha, \beta, \gamma) &= \frac{\sqrt{\alpha}}{2\gamma j} e^{j2\pi\beta\tau} \left( e^{-2\pi \frac{\gamma}{\sqrt{\alpha}}\tau} (E_1(-2\pi z_- \tau) + j2\pi) - e^{2\pi \frac{\gamma}{\sqrt{\alpha}}\tau} E_1(2\pi z_-^* \tau) \right) \\ &= -\frac{\sqrt{\alpha}}{2\gamma} e^{j2\pi\beta\tau} \left( -2\pi e^{-2\pi \frac{\gamma}{\sqrt{\alpha}}\tau} + F(-z_- \tau) - F(z_-^* \tau) \right), \quad \tau \geq 0. \end{aligned} \quad (\text{A.13})$$

Proceeding the analysis in a similar fashion we find that the exponential term in (A.10) cancels out and, for  $0 < f_{max} \leq \beta$

$$I(\tau, \alpha, \beta, \gamma) = \frac{\gamma}{2\sqrt{\alpha}} e^{j2\pi\beta\tau} (F(-z_- \tau) - F(z_-^* \tau) - F(-z_+^* \tau) + F(z_+ \tau)). \quad (\text{A.14})$$

For  $\tau = 0$ , (A.11) remains valid.

## A.3 The case when $\gamma \leq 0$ and/or $\beta < 0$ and/or $\tau < 0$

From the integral definition in (A.1) we see that the sign of  $\gamma$  is immaterial, in other words of  $I(\tau, \alpha, \beta, \gamma) = I(\tau, \alpha, \beta, -\gamma)$ . Therefore, all previous results also apply for  $\gamma < 0$  provided  $\gamma$  is replaced by  $-\gamma$  (or, more conveniently, by  $|\gamma|$ , making the expressions valid for all  $\gamma \neq 0$ ). For  $\gamma = 0$  the integral is zero and the expression also applies. The previous expression also apply when  $\beta < 0$  the results in Subsection A.1 for  $f_{max} > -\beta$  and the results in Subsection A.2 for  $f_{max} < -\beta$ . When  $\tau < 0$  it can be verified that (A.10) yields  $I(-\tau, \alpha, \beta, \gamma) = I^*(\tau, \alpha, \beta, \gamma)$  so it is also valid for negative lags. The only restriction which then remains is  $\alpha > 0$ .

## A.4 Summary

The closed-form expression for the integral  $I(\tau, \alpha, \beta, \gamma)$  obtained in this Appendix is summarized as follows: for any  $\alpha > 0$  (and the trivial condition  $f_{max} > 0$ ) the integral in (A.1) may be

expressed as

$$I(\tau, \alpha, \beta, \gamma) = \begin{cases} \frac{|\gamma|}{2\sqrt{\alpha}} e^{j2\pi\beta\tau} \left[ U \cdot 2\pi e^{-2\pi \frac{|\gamma|}{\sqrt{\alpha}} |\tau|} + F(-z_- \tau) - F(z_-^* \tau) - F(-z_+^* \tau) + F(z_+ \tau) \right], & \tau \neq 0 \\ \frac{\gamma}{\sqrt{\alpha}} \left[ \arctan \left( \sqrt{\alpha} \frac{f_{max} - \beta}{\gamma} \right) + \arctan \left( \sqrt{\alpha} \frac{f_{max} + \beta}{\gamma} \right) \right], & \tau = 0 \end{cases}$$

where  $z_{\pm} \triangleq \frac{|\gamma|}{\sqrt{\alpha}} + j(f_{max} \pm \beta)$  and  $U \triangleq \begin{cases} 1, & f_{max} > |\beta| \\ 0, & f_{max} \leq |\beta| \end{cases}$ . When  $\beta = 0$  this becomes

$$I(\tau, \alpha, 0, \gamma) = \begin{cases} \frac{|\gamma|}{\sqrt{\alpha}} \left[ \pi e^{-2\pi \frac{|\gamma|}{\sqrt{\alpha}} |\tau|} + \Re\{F(-z_0 \tau) + F(z_0 \tau)\} \right], & \tau \neq 0 \\ \frac{2\gamma}{\sqrt{\alpha}} \arctan \left( \sqrt{\alpha} \frac{f_{max}}{\gamma} \right), & \tau = 0 \end{cases}$$

where  $z_0 \triangleq \frac{|\gamma|}{\sqrt{\alpha}} + j f_{max}$ .



## Appendix B – Derivation of series expansion for the LCR

In this Appendix we prove the equality in (11). From (7), the factor  $G(\rho, K, \chi)$  is expressed as

$$G(\rho, K, \chi) \triangleq \frac{2}{\pi} \int_0^{\pi/2} \cosh(a \cos \theta) \left( e^{-\chi^2 \sin^2 \theta} + \sqrt{\pi} \chi \sin \theta \operatorname{erf}(\chi \sin \theta) \right) d\theta \quad (\text{B.1})$$

where  $a \triangleq 2\sqrt{K(K+1)}\rho$ . Expanding both the exponential function and  $\operatorname{erf}(\cdot)$  (see [11, eq. (8.253-1)]) on the second factor of the integrand function as McLaurin series yields

$$\begin{aligned} e^{-\chi^2 \sin^2 \theta} + \sqrt{\pi} \chi \sin \theta \operatorname{erf}(\chi \sin \theta) &= \sum_{n=0}^{\infty} \frac{(-\chi^2 \sin^2 \theta)^n}{n!} + \sqrt{\pi} \chi \sin \theta \underbrace{\frac{2}{\sqrt{\pi}} \sum_{n=0}^{\infty} (-1)^n \frac{(\chi \sin \theta)^{2n+1}}{(2n+1)n!}}_{\operatorname{erf}(\chi \sin \theta)} \\ &= 1 + \sum_{n=1}^{\infty} \frac{(-\chi^2 \sin^2 \theta)^n}{n!} + 2 \sum_{n=0}^{\infty} (-1)^n \frac{(\chi \sin \theta)^{2n+2}}{(2n+1)n!} \\ &= 1 + \sum_{n=1}^{\infty} (-1)^n \frac{(\chi \sin \theta)^{2n}}{n!} + 2 \sum_{n=1}^{\infty} (-1)^{n-1} \frac{(\chi \sin \theta)^{2n}}{(2n-1)(n-1)!} \\ &= 1 + \sum_{n=1}^{\infty} (-1)^{n-1} \frac{(\chi \sin \theta)^{2n}}{n!} \left( -1 + \frac{2n}{2n-1} \right) \\ &= 1 + \sum_{n=1}^{\infty} (-1)^{n-1} \frac{(\chi \sin \theta)^{2n}}{(2n-1)n!}. \end{aligned} \quad (\text{B.2})$$

Substituting (B.2) in (B.1) gives

$$\begin{aligned} G(\rho, K, \chi) &= \frac{2}{\pi} \int_0^{\pi/2} \cosh(a \cos \theta) \left( 1 + \sum_{n=1}^{\infty} (-1)^{n-1} \frac{(\chi \sin \theta)^{2n}}{(2n-1)n!} \right) d\theta \\ &= \frac{2}{\pi} \int_0^{\pi/2} \cosh(a \cos \theta) d\theta + \frac{2}{\pi} \sum_{n=1}^{\infty} (-1)^{n-1} \frac{\chi^{2n}}{(2n-1)n!} \int_0^{\pi/2} \cosh(a \cos \theta) \sin^{2n} \theta d\theta \\ &= I_0(a) + \frac{2}{\pi} \sum_{n=1}^{\infty} (-1)^{n-1} \frac{\chi^{2n}}{(2n-1)n!} \frac{\sqrt{\pi}}{2} \left( \frac{2}{a} \right)^n \Gamma\left(n + \frac{1}{2}\right) I_n(a) \\ &= I_0(a) + \frac{1}{\sqrt{\pi}} \sum_{n=1}^{\infty} (-1)^{n-1} \frac{\Gamma\left(n + \frac{1}{2}\right)}{(2n-1)n!} \left( \frac{2\chi^2}{a} \right)^n I_n(a) \end{aligned} \quad (\text{B.3})$$

where we have used the definite integrals [11, eq. (3.915-4), eq. (8.431-5)] with adequate modification of the integration limits. This proves (11) for  $a > 0$  and any  $\chi \geq 0$ . As  $a \rightarrow 0$ ,  $I_n(a) \rightarrow \frac{(a/2)^n}{n!}$  for all  $n \geq 1$  so  $\frac{I_n(a)}{a^n} \rightarrow 0$ . Thus, for  $a = 0$ ,  $G(\rho, K, \chi) = I_0(0) = 1$  which completes the proof of (11).





# References

- [1] V. Erceg, L. Schumacher, P. Kyritsi, et al., “TGn channel models,” *IEEE 802.11-03/940r4*, May 2004, <https://mentor.ieee.org/802.11/dcn/03/11-03-0940-04-000n-tgn-channel-models.doc>.
- [2] G. Breit, H. Sampath, S. Vermani, et al., “IEEE 802.11 TGac channel model addendum,” *IEEE 802.11-09/308r12*, Mar. 2010, <https://mentor.ieee.org/802.11/dcn/09/11-09-0308-12-00ac-tgac-channel-model-addendum-document.doc>.
- [3] R. Liu, J. Porat, N. Jindal, et al., “IEEE 802.11ax channel model document,” *IEEE 802.11-14/0882r4*, Sept. 2014, <https://mentor.ieee.org/802.11/dcn/14/11-14-0882-04-00ax-tgax-channel-model-document.docx>.
- [4] T. K. Paul and T. Ogunfunmi, “Wireless LAN comes of age: Understanding the IEEE 802.11n amendment,” *Circuits and Systems Magazine, IEEE*, vol. 8, no. 1, pp. 28–54, first quarter 2008.
- [5] K. I. Schumacher, L. Pedersen and P. E. Mogensen, “From antenna spacings to theoretical capacities – guidelines for simulating MIMO systems,” in *Proc. PIMRC Conf.*, Sept. 2002, vol. 2, pp. 587–592.
- [6] M. Abramowitz and I. A. Stegun, *Handbook of Mathematical Functions, With Formulas, Graphs, and Mathematical Tables*, Dover, 1974.
- [7] V. Pegoraro and P. Slusallek, “On the evaluation of the complex-valued exponential integral,” *Journal of Graphics, GPU, and Game Tools*, vol. 15, no. 3, pp. 183–198, 2011.
- [8] L. Schumacher and B. Dijkstra, “Description of a MATLAB implementation of the indoor MIMO WLAN channel model proposed by the IEEE 802.11 TGn channel model special committee,” *Implementation note version 3.2*, May 2004, [https://staff.info.unamur.be/lsc/Research/IEEE\\_80211\\_HTSG\\_CMSC/distribution\\_terms.html](https://staff.info.unamur.be/lsc/Research/IEEE_80211_HTSG_CMSC/distribution_terms.html).

- [9] A. Abdi, K. Wills, H.A. Barger, M.-S. Alouini, and M. Kaveh, “Comparison of the level crossing rate and average fade duration of Rayleigh, Rice and Nakagami fading models with mobile channel data,” in *52nd Vehicular Technology Conference, 2000. IEEE-VTS Fall VTC 2000*, Sept. 2000, vol. 4, pp. 1850–1857.
- [10] M. Patzold, U. Killat, and F. Laue, “An extended Suzuki model for land mobile satellite channels and its statistical properties,” *Vehicular Technology, IEEE Transactions on*, vol. 47, no. 2, pp. 617–630, May 1998.
- [11] I.S. Gradshteyn and I.M. Ryzhik, *Table of Integrals, Series and Products*, Academic Press, 5th edition, 1994.
- [12] Konrad Knopp and Frederick Bagemihl, *Infinite Sequences and Series*, Dover publications, New York, 1956.
- [13] D. Rainville, *Infinite Series*, Macmillan, 1967.
- [14] “NIST Digital Library of Mathematical Functions,” <http://dlmf.nist.gov/> Release 1.0.10 of 2015-08-07, Online companion to [17].
- [15] N. N. Lebedev, *Special Functions and Their Applications*, Dover, 1972.
- [16] F. W. J. Olver, “Uniform, exponentially improved, asymptotic expansions for the generalized exponential integral,” *SIAM J. Math. Anal.*, vol. 22, no. 5, pp. 1460–1474, Sept. 1991.
- [17] F. W. J. Olver, D. W. Lozier, R. F. Boisvert, and C. W. Clark, Eds., *NIST Handbook of Mathematical Functions*, Cambridge University Press, New York, NY, 2010, Print companion to [14].